From Transient to Stationary Transport in Porous Networks under Various Adsorption Conditions and Kinetics

Daniela Bauer, Zaineb Zaafouri, Guillaume Batôt, Benoit Coasne

From Transient to Stationary Transport in Porous Networks under Various Adsorption Conditions and Kinetics

Daniela Bauer,*,† Zaineb Zaafouri,† Guillaume Batôt,† and Benoit Coasne‡

† *IFP Energies Nouvelles, 1 & 4 Av. Bois Préau, 92852 Rueil Malmaison, France*
‡*Université Grenoble Alpes, CNRS, LIPhy, 38000 Grenoble, France*

E-mail: daniela.bauer@ifpen.fr

Abstract

We investigate the interplay between adsorption and transport in a two-dimensional porous medium by means of an extended Lattice Boltzmann technique within the Two-Relaxation-Time framework. We focus on two canonical adsorption thermodynamics and kinetics formalisms: (1) the Henry model in which the adsorbed amount scales linearly with the free adsorbate concentration and (2) the Langmuir model that accounts for surface saturation upon adsorption. We simulate transport of adsorbing and non-adsorbing particles to investigate the effect of the adsorption/desorption ratio k, initial free adsorbate concentration c_0, surface saturation Γ^∞ and Peclet numbers Pe on their dispersion behavior. In all cases, despite marked differences between the different adsorption models, the three following transport regimes are observed: diffusion-dominated regime, transient regime and Gaussian or nearly Gaussian dispersion regime. On the one hand, at short times, the intermediate transient regime strongly depends on the system's parameters with the shape of the concentration field at a given time being dependent on the amount of particles adsorbed shortly after injection. On the other hand, at longer times, the influence of the initial condition attenuates as particles sample sufficiently the adsorbed and non-adsorbed states. Once such dynamical equilibrium is reached, transport becomes Gaussian (i.e. normal) or nearly Gaussian in the asymptotic regime. Interestingly, the characteristic timescale to reach equilibrium, which varies drastically with the system's parameters, can be much longer than the actual simulation time. In practice, such results reflect many experimental situations such as in water treatment where dispersion is found to remain anomalous (non-Gaussian) even if transport is considered over long macroscopic times.

1 Introduction

Despite being a very old research problem, transport in porous media remains a vivid field as scientists keep unveiling novel phenomena that pertain to both basic and practical science. In particular, with the advent of nanotechnologies (e.g. nanofluidics, nanoporous solids), many complex mechanisms have been identified as resulting from the thermodynamics/dynamics interplay of fluids confined at the nanometer scale or near surfaces. While such effects are prominent in nanofluidic channels or nanoporous media, it is acknowledged that they also apply in larger pores as such coupling always occurs at surfaces with strong impact on macroscopic properties. Of particular relevance, beyond well-known aspects relevant to the thermodynamics of confinement (condensation, drying, cavitation, etc.), adsorption effects are known to strongly affect the diffusion and transport of fluids in restricted geometries.[1–11]

Among important problems in this field, the case of a flowing liquid (solvent) that carries adsorbable particles (solute) in a porous solid has been considered extensively.[12,13] Formally, such situations corresponding to dispersion upon the combined effect of advection and adsorption can be treated by considering available formalisms from statistical physics (e.g. Fokker-Planck equation, intermittent Brownian motion) or continuum-level approaches (e.g. adsorption-advection-diffusion equation, Taylor dispersion with adsorption/desorption). Numerically, such problems can be tackled by employing existing frameworks such as Lattice Boltzmann calculations, continuous time random walk strategies, and network models. In particular, for all these different approaches, several extensions have been proposed to account for adsorption effects which affect the dispersion and flow of molecules in porous networks.

Most available works using the strategies above consider dispersion upon advection and adsorption under static conditions (stationary flow). Yet, in many practical situations, transient regimes are observed as adsorption effects and associated surface residence times induce strong dynamics heterogeneities that lead to non-conventional behaviors. Typically, such transient dynamics are seen at times shorter than the time required to reach local equilibrium between the adsorbed and free molecules concentrations. Understanding such complex dynamics requires to unravel the coupling between molecule transport and adsorption kinetics near surfaces by integrating the latter into transport models. Such integration allows describing rigorously the combination of mass transfer, diffusion, and adsorption. The morphology and topology of the host porous network is another key ingredient that drastically affects transport (in particular, both adsorption and transport are directly impacted by the geometry of the solid/liquid interface).[14–16] In this context, solid properties such as necks or low porosity regions induce a strong coupling between transport and adsorption.[8,17,18]

Beyond such adsorption kinetic effects, transient regimes can be observed even at times much larger than the typical time to reach adsorption/desorption thermodynamic equilibrium. Indeed, depending on the adsorption/desorption turnover frequency ν, the concentration field of adsorbable molecules will obey one of the two following asymptotic regimes. By describing each particle's trajectory as subsequent surface residence steps and relocation steps through the porosity, we can introduce t_A and t_B the characteristic residence and relocation times (with this convention, the adsorption/desorption turnover frequency is simply $\nu \sim [t_A + t_B]^{-1}$). (1) In the long time range ($t >> t_A,\ t_B$), transport appears stationary with an underlying Gaussian propagator $P(r,t)$; in this case, every particle undergoes many residence and relocation steps, therefore leading to homogeneous transport properties. (2) In the short time range ($t << t_A,\ t_B$), the transport is non-stationary with a strongly asymmetrical (i.e. non-Gaussian) propagator $P(r,t)$; in this case, overall transport appears as the sum of two drastically different transport types corresponding to adsorbed and non-adsorbed molecules that do not exchange. Between these two extreme limits, transport evolves in time with a non-Gaussian propagator that becomes more and more symmetrical with increasing time due to increasing exchange between adsorbed and non-adsorbed molecules. Interestingly, while the transport is usually assumed to be stationary in the literature, the preasymptotic, i.e. non-stationary, regime can extend to very long times that go well beyond the characteristic time probed in existing approaches. In particular, in disordered porous media, the resulting heterogeneous flow properties combined with broad distributions of adsorption/desorption times can lead to very complex effects that challenge existing theoretical frameworks.

In order to provide a better understanding of transport in porous media of adsorbable particles, we report here Lattice Boltzmann calculations to investigate the time behavior of transport under different adsorption conditions and kinetics. With this goal, we use a Lattice Boltzmann scheme extended to account for both adsorption thermodynamics and kinet-

ics.[19] Such a Lattice Boltzmann scheme, which enables running massively parallel calculations that span large length and time scales, is suitable to decipher adsorption-induced effects in both transient and stationary transport regimes in porous structures. All simulations are conducted using a Lattice Boltzmann approach within the Two Relaxation Time framework; this formalism allows one to obtain accurate and stable data even when complex porous materials are considered. Two characteristic adsorption thermodynamics/kinetics – which pertain to a very large number of situations encountered in fundamental and practical science – are considered: Henry and Langmuir adsorption. Using a prototypical system corresponding to a simple yet representative model of connected porous media, we investigate the coupling between the injection boundary condition (initial concentration) and the adsorption kinetics (adsorption/desorption ratio, surface saturation) and its influence on the transient and stationary transport responses. The remainder of this paper is structured as follows. In Section 2, we introduce the different adsorption kinetics and provide the main ingredients of the extended Lattice Boltzmann scheme employed here (all details can be found in the Supplemental Information file). We also describe the 2D porous structure considered in this paper and the resulting Stokes velocity field obtained using conventional Lattice Boltzmann calculations. In Section 3, we present our results obtained for transport induced upon Dirac pulse injection. For both Henry and Langmuir adsorption, we focus on the influence on transport of the initial concentration and surface saturation in combination with different adsorption/desorption ratios on transport. Additionally, we consider the influence of the Peclet number. Section 4 provides some concluding remarks and suggestions for future work.

2 Methods

2.1 Advection, diffusion and adsorption

Transport of adsorbable molecules is classically described by the advection-diffusion-adsorption equation:

$$\frac{\partial c(\mathbf{r},t)}{\partial t} + \mathbf{u}\cdot\nabla c(\mathbf{r},t) - \nabla\cdot[D_m\nabla c(\mathbf{r},t)] + \frac{\partial c_a(\mathbf{r},t)}{\partial t} = 0 \quad (1)$$

Here, $c(\mathbf{r},t)$ and $c_a(\mathbf{r},t)$ represent the free and adsorbed particle concentrations, respectively. $\mathbf{u}$ is the local Stokes flow velocity and D_m stands for the molecular self-diffusivity of the free particles. The adsorbed amount Γ – which corresponds to a surface density – is related to the volume concentration c_a of adsorbed molecules as $\Gamma = c_a l$ (where $l = \Delta x$ is the unit length of the lattice site in Lattice Boltzmann calculations). Specific adsorption kinetics characterize the relation between Γ and the volume concentration c of free particles under non-equilibrium and equilibrium conditions. In this paper, we focus on two classical adsorption kinetics resulting in the so-called Henry and Langmuir adsorption isotherms.

Henry adsorption. With this model, the adsorbed amount Γ is proportional to the bulk adsorbate concentration c with an underlying adsorption kinetics given by:

$$\frac{\partial\Gamma}{\partial t} = k_A c\Gamma^0 - k_D\Gamma \quad (2)$$

where k_A and k_D represent the adsorption and desorption rates while Γ^0 is a characteristic adsorbed amount. Solving Eq. 2 leads to $\Gamma(t) = \Gamma^0[1 - e^{-k_D t}]k_H c$ with $k_H = k_A/k_D$. At equilibrium, for $t \to \infty$, the Henry adsorption isotherm writes $\Gamma(t) = \Gamma^0 k_H c$.

Langmuir adsorption. This model is based on the assumption of molecules being adsorbed on specific sites at the surface of the adsorbent (all sites are assumed to be identical). Only one molecule can be adsorbed in each site so that a single monomolecular adsorbed layer can

form (surface saturation property). The dynamical equilibrium between adsorbed and free molecules is given by the following kinetic equation:

$$\frac{\partial \Gamma}{\partial t} = k_A c(\Gamma^\infty - \Gamma) - k_D \Gamma \qquad (3)$$

where Γ^∞ corresponds to surface saturation. Solving the latter equation leads to $\Gamma(t) = [1 - e^{-k_D(1+k_L c)t}]\Gamma^\infty k_L c/(1+k_L c)$ with $k_L = k_A/k_D$. At equilibrium, for $t \to \infty$, the Langmuir adsorption isotherm writes $\Gamma(t) = \Gamma^\infty k_L c/[1 + k_L c]$.

2.2 Lattice Boltzmann scheme

Transport of adsorbable particles was simulated by means of a recently developed Lattice Boltzmann scheme (which was validated for a simple slit pore geometry against the analytical solution given in[20]). A complete discussion including full validation can be found in.[19] Lattice Boltzmann simulations consist in two steps.

• First, after specifying the porous medium geometry, the Stokes flow of the carrier fluid is independently computed by means of a simple Lattice Boltzmann scheme. Information on such a classical Lattice Boltzmann scheme for the resolution of Stokes equation is given in the Supplemental Information. In our approach, we assume that the velocity field of the carrier fluid is not modified upon adsorption. Fig. 1 [Top] shows the regular porous structure for which the present simulation work was conducted. Using a regular porous structure allows us to disentangle flow heterogeneity effects and adsorption effects on macroscopic transport. The velocity field computed by solving Stokes equation is also given in Fig. 1 [Bottom right].

• Second, transport of adsorbable particles is simulated. The simulations start with the injection of molecules at a specific time $t = 0$ and position x_0 (x is the direction parallel to the flow). In the present work, we consider pulse (Dirac) injections. Using this initial condition, we compute the transport of the adsorbable particles in the porous structure shown in Fig. 1. In the following section, we present the computational details which allow accounting for adsorption kinetics in the transport of adsorbable particles.

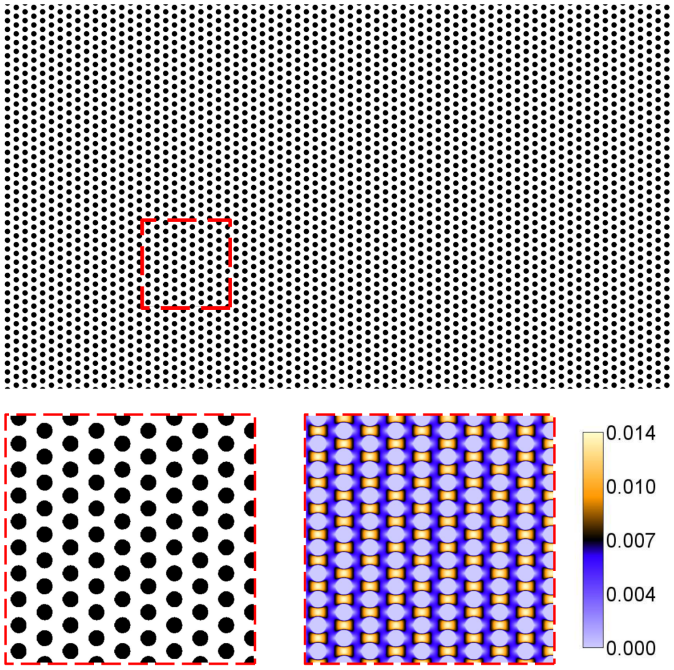

Figure 1: Structural model of the porous medium used in this study. The full two-dimensional geometry of size 2300×4000 Δx^2 is shown in the upper image [Top] with a zoom of size 500×500 Δx^2 [Bottom left]. Stokes velocity field (given in $\Delta x/\Delta t$ units) computed by means of Lattice Boltzmann calculations is also represented [Bottom right]. Δx is the unit length of a lattice site while Δt the unit time step.

2.3 Extended Lattice Boltzmann scheme: Transport and adsorption kinetics

The extended Lattice Boltzmann scheme consists in performing three substeps successively at every time step Δt: *collision*, *adsorption*, and *propagation*. The collision and propagation steps, which are standard steps in Lattice Boltzmann schemes, only apply to the free particle concentration $c(\mathbf{r}, t)$. On the other hand, the adsorption step modifies both the free ($c(\mathbf{r}, t)$) and adsorbed ($c_a(\mathbf{r}, t)$) particle concentrations as it simulates the redistribution kinetics between $c(\mathbf{r}, t)$ and $c_a(\mathbf{r}, t)$. As shown in the following, $c(\mathbf{r}, t)$ is linked to the distribution

$g_q(\mathbf{r},t)$ where $g_q(\mathbf{r},t)$ corresponds to the particle distribution of free particles at time t and position $\mathbf{r}$ having a velocity $\mathbf{v}_q$ in the direction q. The Lattice Boltzmann substeps (collision, propagation, adsorption) are applied to these distributions. We use the D2Q9 mesh for our simulations so that the velocity set consists of four "diagonal" velocities $\mathbf{v}_q = (\pm 1, \pm 1)$, four "coordinate" velocities $\mathbf{v}_q = (\pm 1, 0), (0, \pm 1)$ and the immobile (zero) velocity. The velocity components are denoted as $\mathbf{v}_q$ with $q \in \{0, .., q_m = 8\}$.

The free particle distributions obtained after the propagation, collision and adsorption steps are defined as $g_q(\mathbf{r},t)$, $\tilde{g}_q(\mathbf{r},t)$ and $\tilde{\tilde{g}}_q(\mathbf{r},t)$, respectively. Considering that the latter distributions are normalized, the free particle concentrations after the collision, adsorption, and propagation steps are given by: $\tilde{c}(\mathbf{r},t) = \sum_q \tilde{g}_q(\mathbf{r},t)$, $\tilde{\tilde{c}}(\mathbf{r},t) = \sum_q \tilde{\tilde{g}}_q(\mathbf{r},t)$, and $c(\mathbf{r},t) = \sum_q g_q(\mathbf{r},t)$. For specific reasons detailed below, it is not necessary to introduce distributions for the adsorbed molecules. Indeed, density conservation provides a direct relation between the adsorbed c_a and free c concentrations. During the collision/propagation steps, the q-components $g_q(\mathbf{r},t)$ of the distribution $g(\mathbf{r},t)$ are redistributed. However, their fraction $\tilde{x}_q(\mathbf{r},t) = \tilde{g}_q(\mathbf{r},t)/\tilde{c}(\mathbf{r},t) = \tilde{g}_q(\mathbf{r},t)/\sum_q \tilde{g}_q(\mathbf{r},t)$ is not modified during the adsorption step [i.e. $\tilde{x}_q(\mathbf{r},t) = \tilde{\tilde{x}}_q(\mathbf{r},t)$]. The latter condition is based on the assumption that the velocity distribution $\mathbf{v}_q$ amid the components q is not altered by the adsorption step in spite of the modification of the total number of free particles within one time step Δt, i.e. $\Delta c(\mathbf{r},t) = -\Delta c_a(\mathbf{r},t)$. Here, Δ stands for the difference taken between the collision step $\tilde{}$ and the adsorption step $\tilde{\tilde{}}$. This approximation can be explained by the fact that all particles are adsorbed with the same adsorption rate – independently of their velocity. Consequently, it stands for the fact that all desorbed particles are reintroduced in the population of the free particles according to a velocity distribution verifying the current distribution of q-components.

• **Collision**. In order to mimic collisions, at each time step t and position $\mathbf{r}$, the components $g_q(\mathbf{r},t)$ are redistributed among the site populations:[21,22]

$$\tilde{g}_q(\mathbf{r},t) = \Omega[g(\mathbf{r},t)]_q. \tag{4}$$

Here, $g(\mathbf{r},t)$ represents the set of q-components $g_q(\mathbf{r},t)$ while $\Omega[g(\mathbf{r},t)]_q$ denotes the collision operator transferring momentum between the q-components. In the Two-Relaxation-Time method (TRT), the collision operator involves specific relaxation rates for the anti-symmetric and symmetric components. The anti-symmetric and symmetric components are defined as $g_q^- = (g_q - g_{\bar{q}})/2$ and $g_q^+ = (g_q + g_{\bar{q}})/2$ for $q \in \{1, ..., q_m/2\}$ (for $q = 0$, we have $g_0^+ = g_0$ and $g_0^- = 0$). In the TRT scheme, the update rule for the anti-symmetric and symmetric equilibrium components $e_q^{\pm}$ depends on two relaxation parameters: λ^- for all anti-symmetric non-equilibrium components $n_q^- = g_q^- - e_q^-$ and λ^+ for all symmetric non-equilibrium components $n_q^+ = g_q^+ - e_q^+$. Moreover, $e_0^+ = e_0$ and $e_0^- = 0$ are defined for the zero velocity. The collision update rule applied to $q \in \{1, .., q_m/2\}$ then becomes:[23]

$$\begin{aligned} \tilde{g}_q(\mathbf{r},t) &= g_q(\mathbf{r},t) + \lambda^+ n_q^+ + \lambda^- n_q^- \\ \tilde{g}_{\bar{q}}(\mathbf{r},t) &= g_{\bar{q}}(\mathbf{r},t) + \lambda^+ n_q^+ - \lambda^- n_q^- \\ \tilde{g}_0(\mathbf{r},t) &= g_0(\mathbf{r},t)\ (1+\lambda^+) - \lambda^+ e_0 \end{aligned} \tag{5}$$

The equilibrium components for the D2Q9 scheme are given by:[23]

$$\begin{cases} e_q^+(\mathbf{r},t) = c(\mathbf{r},t) E_q^+ \\ e_q^-(\mathbf{r},t) = c(\mathbf{r},t) E_q^- \\ e_0^+(\mathbf{r},t) = e_0 = c(\mathbf{r},t) E_0 \\ e_0^-(\mathbf{r},t) = 0 \end{cases} \tag{6}$$

with

$$\begin{cases} E_q^+ = t_q^* v_e + \dfrac{t_q^*}{2}[3(\mathbf{u}\cdot\mathbf{v}_q)^2 - \mathbf{u}^2] \\ E_q^- = t_q^*(\mathbf{u}\cdot\mathbf{v}_q) \\ E_0 = 1 - \displaystyle\sum_{q=1}^{q_m} E_q^+(\mathbf{r},t) \end{cases} \tag{7}$$

with $v_e = (D_{xx} + D_{yy})/2$. $t_q^* = \{1/3; 1/12\}$

are the isotropic weights and $\mathbf{u} = \{u_x, u_y\}$ represents the advective velocity ($\mathbf{u}^2 = u_x^2 + u_y^2$). The diffusion coefficients are set to $D_{xx} = D_{yy} = D_m/\Lambda^-$.

The numerical parameters $\Lambda^\pm$ and Λ must be correctly chosen in order to reduce the numerical error and to ensure numerical stability. These parameters and the relaxation constants $\lambda^\pm$ are linked as follows:[23]

$$\begin{cases} \Lambda = \Lambda^+\Lambda^- \\ \Lambda^\pm = -(1/2 + 1/\lambda^\pm) \text{ for } -2 < \lambda^\pm < 0 \end{cases} \quad (8)$$

In this work, we use $\Lambda^+ = 4$ and $\Lambda^- = 1/16$. The velocity field $\mathbf{u}$ results from the Stokes simulation. At the end of this step, the local free particle concentration can be computed from: $\tilde{c}(\mathbf{r}, t) = \sum_q \tilde{g}_q(\mathbf{r}, t)$.

• **Adsorption**. The numerical adsorption step depends on the underlying kinetics. Specific numerical formulations are described in the following section whereas the general formalism is detailed here. The adsorption step follows the first order kinetic equation leading to the adsorption isotherm. Starting from the free and adsorbed particle concentrations [$\tilde{c}(\mathbf{r}, t)$ and $\tilde{c}_a(\mathbf{r}, t)$] resulting at time t from the collision step, the adsorption step provides updated concentrations $\tilde{\tilde{c}}(\mathbf{r}, t)$ and $\tilde{\tilde{c}}_a(\mathbf{r}, t)$. As already mentioned, we assume that $\tilde{\tilde{x}}_q$ (distribution ratio between the different q-components) is not modified by the adsorption step. Based on the definition of the concentration [$\tilde{\tilde{c}}(\mathbf{r}, t) = \sum_q \tilde{\tilde{g}}_q(\mathbf{r}, t)$], we opt for the proportional and homogeneous redistribution between the $\tilde{\tilde{g}}_q$ components of the variation induced by the adsorption operator $A(\tilde{c}, \tilde{c}_a) = \Delta c(\mathbf{r}, t) = \tilde{\tilde{c}}(\mathbf{r}, t) - \tilde{c}(\mathbf{r}, t)$. Thus, after the adsorption step, the particle distribution $\tilde{\tilde{g}}_q(\mathbf{r}, t)$ follows the following evolution equation:

$$\tilde{\tilde{g}}_q(\mathbf{r}, t) = \tilde{g}_q(\mathbf{r}, t) - \tilde{x}_q(\mathbf{r}, t) A(\tilde{c}, \tilde{c}_a) \quad (9)$$

Here $\tilde{x}_q(\mathbf{r}, t) = \tilde{g}_q(\mathbf{r}, t)/\tilde{c}(\mathbf{r}, t)$ represents the particle fraction following a velocity set $\mathbf{v}_q$ at position $\mathbf{r}$ and time t. Specific expressions for the adsorption operator $A(\tilde{c}, \tilde{c}_a)$ for each adsorption isotherm model will be detailed in the final paragraph of this methods section.

• **Propagation**. At each time step t, following the intermediate collision/adsorption substeps, the distribution components $\tilde{\tilde{g}}_q(\mathbf{r}, t)$ are redistributed between their neighboring sites.[21,22] The modification in free particle distribution during the propagation step is given by:

$$g_q(\mathbf{r} + \mathbf{v}_q \Delta t, t + \Delta t) = \tilde{\tilde{g}}_q(\mathbf{r}, t) \quad (10)$$

Here, the particle distributions $\tilde{\tilde{g}}_q(\mathbf{r}, t)$ are displaced according to the velocity set $\{\mathbf{v}_q\}$. Thus, particles located at time t in node $\mathbf{r}$ are transferred to $\mathbf{r} + \mathbf{v}_q \Delta t$ at the end of the iteration step.

2.4 Numerical scheme for adsorption kinetics

The adsorption step is based on the specific first order kinetic equation leading to the adsorption isotherm at equilibrium (Henry and Langmuir adsorption models in the present work). For each model, the variation of $c(\mathbf{r}, t)$ and $c_a(\mathbf{r}, t)$ depends on the specific underlying kinetics equation. In practice, the free and adsorbed particle concentrations [$\tilde{\tilde{c}}(\mathbf{r}, t)$ and $\tilde{\tilde{c}}_a(\mathbf{r}, t)$] are computed from the concentrations [$\tilde{c}(\mathbf{r}, t)$ and $\tilde{c}_a(\mathbf{r}, t)$] obtained after the collision step using the kinetic equations presented in what follows.

Henry adsorption. Numerical equations for the Henry adsorption kinetics can be written as:

$$\tilde{\tilde{c}}_a(\mathbf{r}, t) = p_A \tilde{c}(\mathbf{r}, t) + [1 - p_D] \tilde{c}_a(\mathbf{r}, t) \quad (11)$$

$$\tilde{\tilde{c}}(\mathbf{r}, t) = \tilde{c}(\mathbf{r}, t) - p_A \tilde{c}(\mathbf{r}, t) + p_D \tilde{c}_a(\mathbf{r}, t) \quad (12)$$

Here, p_A and p_D represent the adsorption and desorption rates in Lattice Boltzmann units $(\Delta x, \Delta t)$, respectively. p_A and p_D are related to the physical adsorption and desorption rates as $p_A = k_A \Delta t/\Delta x$ and $p_D = k_D \Delta t$.

Langmuir adsorption. Surface saturation is the main specificity of this adsorption model. Such feature implies that the adsorbed concentration $c_a(\mathbf{r}, t)$ is at all times lower than c_a^∞ – a specific surface concentration that is an intrinsic property of the fluid/solid couple under study. The numerical equations of the Lang-

muir adsorption model are given by:

$$\tilde{\tilde{c}}_a(\mathbf{r},t) = p_A \tilde{c}(\mathbf{r},t)\left[1 - \frac{\tilde{c}_a(\mathbf{r},t)}{c_a^\infty}\right] + (1-p_D)\tilde{c}_a(\mathbf{r},t) \quad (13)$$

$$\tilde{\tilde{c}}(\mathbf{r},t) = \tilde{c}(\mathbf{r},t) - p_A \tilde{c}(\mathbf{r},t)\left[1 - \frac{\tilde{c}_a(\mathbf{r},t)}{c_a^\infty}\right] + p_D \tilde{c}_a(\mathbf{r},t) \quad (14)$$

Here, the maximum surface concentration can be written as $\Gamma^\infty = c_a^\infty \Delta x$ with p_A and p_D defined like for the Henry model: $p_A = k_A \Delta t/\Delta x$ and $p_D = k_D \Delta t$.

3 Results

Adsorption and transport in porous media can be characterized efficiently by monitoring the time evolution of the concentration field and propagators (i.e. particle displacement distributions). In particular, the second moment of the concentration distribution, which corresponds to the displacement variance $\sigma_x^2(t) = \langle[x - \langle x\rangle]^2\rangle$ along the flow direction x, allows computing the dispersion coefficient $D(t) = \mathrm{d}\sigma_x^2(t)/2\mathrm{d}t$. In the long time limit, $D(t)$ becomes constant at the plateau value defined as the effective dispersion coefficient $D_{eff} = \lim_{t\to\infty} \mathrm{d}\sigma_x^2(t)/2\mathrm{d}t$ with an underlying symmetrical concentration field. The dimensionless third moment – the so-called skewness $\gamma = \langle[x - \langle x\rangle]^3\rangle/\sigma^3$ – provides further information on anomalous transport as it characterizes the asymmetry of the concentration field. While $\gamma > 0$ indicates that the concentration peak is located at smaller values than the mean displacement $\langle x\rangle$, $\gamma < 0$ corresponds to "tailing" as the concentration peak is located at larger values than the mean displacement $\langle x\rangle$. In other words, for $\gamma > 0$, many particles are retained due to surface adsorption or confinement effects with a smaller fraction following fast streamlines in the Stokes flow field. In contrast, for $\gamma < 0$, most molecules are dispersed along the Stokes flow field while only a small particle fraction is retarded due to adsorption. Schematic concentration fields obtained for $\gamma > 0$, $\gamma < 0$ and $\gamma = 0$ are illustrated in Fig. 2. As another key descriptor, the Peclet number represents the ratio of transfer due to advection and transfer due to diffusion: $Pe = \bar{u}d/D_m$ where $\bar{u}$ is the average flow velocity and d a characteristic size (e.g. pore size, pore throat). In what follows, we consider the transport of particles in the porous structure shown in Fig. 1. We first present the results obtained for particles adsorbing according to the Henry adsorption isotherm. Then, we present the results obtained for the dispersion and transport of particles obeying the Langmuir adsorption model.

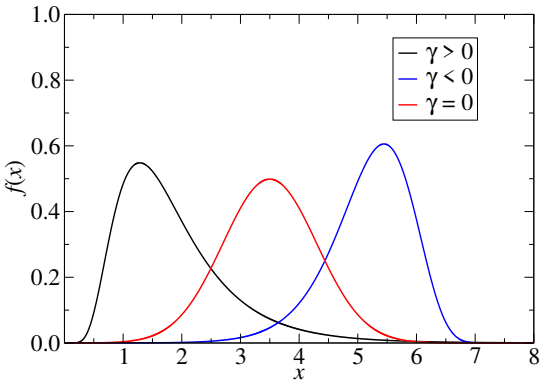

Figure 2: Skewness for different concentration fields

3.1 Henry adsorption model

3.1.1 Adsorption/desorption ratio k_H

Using the Henry adsorption model, we investigate the transport behavior of particles for different adsorption/desorption ratios k_H. In all cases, except if stated otherwise, the initial concentration and Peclet number are $c_0 = 10$ and $Pe = 19$. In practice, k_H is varied in the range of $[0, 1000]$ while keeping the desorption ratio constant $k_D = 0.001$. Fig. 3 [Top] shows the normalized dispersion coefficient $D(t)/D_m$ where D_m is the molecular coefficient that drives the diffusion of particles in the short time scale. For all k_H, three distinct transport regimes are observed when plotting $D(t)$ as a function of time t: molecular diffusion in the short time range, advection-dominated

transport in the intermediate time range, and effective (Taylor) dispersion in the long time range. This result is in agreement with our previous work in which dispersion in simple channels with adsorbing conditions was found to display the same three regimes.[19,24] Fig. 3 shows that $D(t)/D_m$ reaches a plateau after a characteristic time scale that increases drastically with increasing k_H (note the use of a log scale for the time axis). Such a result can be rationalized by invoking the adsorption/desorption turnover frequency ν which decreases with increasing k_H. Considering that Gaussian transport is obtained when all particles have sufficiently exchanged between the adsorbed and free phases, the plateau regime corresponding to effective dispersion is reached at increasing times with increasing k_H.

Upon looking at transient regimes (intermediate time range), significant differences are observed between the data obtained at various k_H. A maximum in $D(t)/D_m$ is observed at large k_H while $D(t)/D_m$ evolves in time without showing large variations. As shown in[24] for a simple channel geometry, such a maximum results from the use of adsorption conditions without surface saturation (i.e. Henry regime). Such unrestricted adsorption leads to the adsorption (i.e. retention) of a very large amount of particles rapidly after the concentration pulse injection. In turn, when probing particle displacements, $D(t)/D_m$ exhibits a maximum in the intermediate time range as it combines two subpopulations with drastically different underlying concentration fields: (1) particles that are not yet adsorbed and directly transported by the Stokes velocity field and (2) particles strongly adsorbed in the injection region with almost no advective transport. This interpretation is confirmed by the concentration profiles in Fig. 3 [Bottom] where the bulk concentration is found to be very small for large k_H but large for small k_H. In contrast, as expected, in the long time limit, significant exchange between the adsorbed and free phases occurs so that the two subpopulations become indistinguishable with a single effective dispersion coefficient that reflects both the adsorption condition k_H and pore network morphology. Interestingly, as shown in Fig. 4, the normalized effective dispersion coefficient D_{eff}/D_m increases with k_H for $k_H < 20$ and then decreases upon further increasing k_H. Such a non-monotonous behavior can be rationalized as follows. On the one hand, for small k_H, D_{eff}/D_m increases with increasing k_H as stronger retention effects through adsorption at the surface leads to more and more drastic differences between the slow adsorbed phase and fast diffusive/advective phase. On the other hand, for large k_H, while strong adsorption effects still induce large differences in the transport properties of the adsorbed and free phases, the dispersion coefficient in the long time limit decreases with k_H as the increasing adsorption strength leads to slower effective diffusion. Therefore, the maximum observed in $D(t)/D_m$ can be rationalized by considering the combined impact of the two following competing effects. (1) Increasing k_H induces strong retention at the surface which leads to overall reduced transport properties (as reflected by the small effective dispersion coefficient obtained for large k_H). (2) Increasing k_H leads to drastic differences in the transport of the adsorbed and free phases which lead to a large dispersion coefficient (as the latter reflects in an average, effective fashion the properties of the slow and fast populations).

Fig. 5 shows the skewness γ as a function of k_H after 5×10^5 timesteps. The insert also shows the temporal evolution of the skewness for $k_H = 2$, $k_H = 20$, $k_H = 50$. To provide further insights, Fig. 6 presents the propagators – i.e. the displacement distributions $P(x,t)$ – obtained for the same k_H at $t = 4 \times 10^4 \Delta t$, $10^5 \Delta t$ and $5.8 \times 10^5 \Delta t$. Upon increasing k_H, the skewness γ increases from an asymptotic negative value for $k_H = 0$ to positive values for large k_H. Such behavior can be rationalized by taking into consideration the competition between tortuosity effects (flow path heterogeneities, dominant at low k_H) and adsorption effects (retention time at the solid surface, dominant at large k_H). For $k_H = 0$, the skewness γ is slightly negative as the intrinsic tortuosity of the host porous structure induces heterogeneous flow paths. Under such non-adsorbing conditions, most particles are transported along

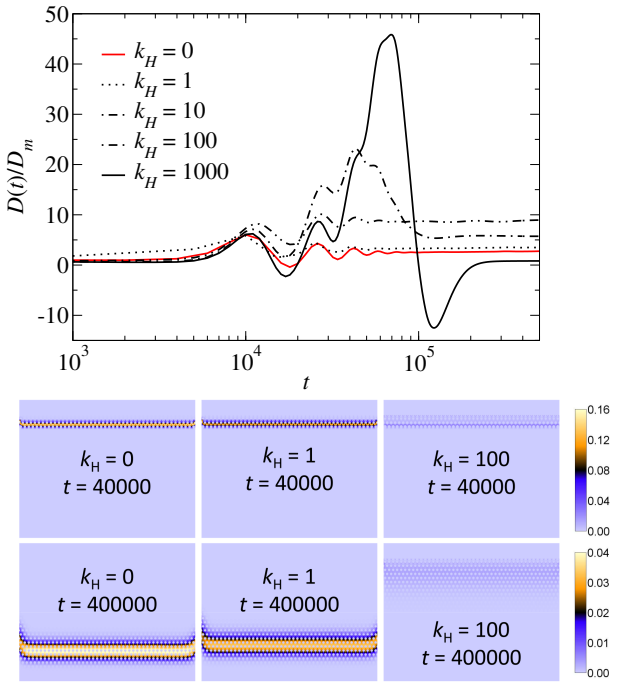

Figure 3: [Top] Dispersion coefficient $D(t)$ normalized by the molecular diffusion coefficient D_m of the free, i.e. non-adsorbing, particles. Particles adsorb according to a Henry adsorption model with different adsorption/desorption rates k_H. The red line corresponds to data for non-adsorbing conditions. The initial concentration is $c_0 = 10$ and the Peclet number $Pe = 19$. [Bottom] Concentration profiles at $t = 4 \times 10^4$ and $t = 4 \times 10^5$ for $k_H = 0$, $k_H = 1$ and $k_H = 100$.

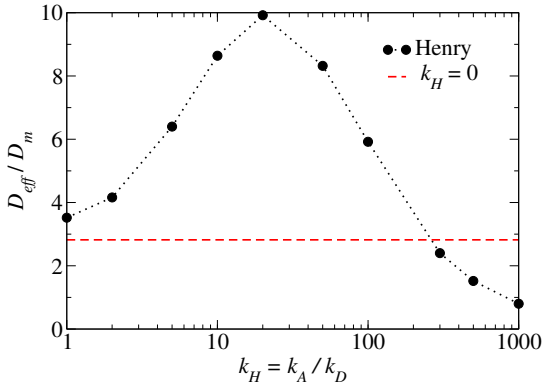

Figure 4: Normalized effective dispersion coefficient D_{eff}/D_m for particles following a Henry adsorption isotherm for different k_H. The red line corresponds to data for non-adsorbing conditions when $k_H = 0$. In all cases, the initial concentration is $c_0 = 10$ and the Peclet number is $Pe = 19$.

the main streamlines but a non-negligible part follows a distribution of slow paths which lead to a negative skewness (tailing). For small k_H (e.g. $k_H = 2$), γ remains strictly negative but increases (i.e. becomes less negative) upon increasing k_H due to adsorption effects. Under such weakly adsorbing conditions, heterogeneities in flow paths remain predominant but non-negligible adsorption of the particles attenuates flow heterogeneities as many particles get delayed due to retention at the solid surface. As k_H keeps increasing, the skewness becomes positive as adsorption effects become predominant over flow heterogeneities. Under such strongly adsorbing conditions, most particles are retained at the solid surface with a small yet noticeable fraction of particles following the flow paths without being adsorbed. Such a situation $\gamma > 0$, which can be seen as symmetrical of the situation $\gamma < 0$ observed for weakly adsorbing conditions, corresponds to anti-tailing of the displacement distribution $P(x,t)$.

As shown in the insert in Fig. 5, upon increasing the time t, the skewness $\gamma(t)$ converges towards zero as the propagator reaches a quasi-Gaussian shape. In fact, γ remains negative until the normalized dispersion coefficient $D(t)/D_m$ reaches its maximum and increases with positive values until $D(t)/D_m$ reaches its minimum. Then, for longer times, γ should decrease towards a final value corresponding to zero as all particles alternate between the adsorbed and non-adsorbed states until reaching dynamic equilibrium. However, in practice, with our simulation setup, such dynamical equilibrium is only attained for systems larger than the present porous structure considered here so that γ remains positive at the maximum time. The propagators $P(x,t)$ (considered at different times in Fig. 6) show the typical shape of positive/negative skewness where the maximum of the displacement distribution is situated either at smaller or larger x than the mean displacement.

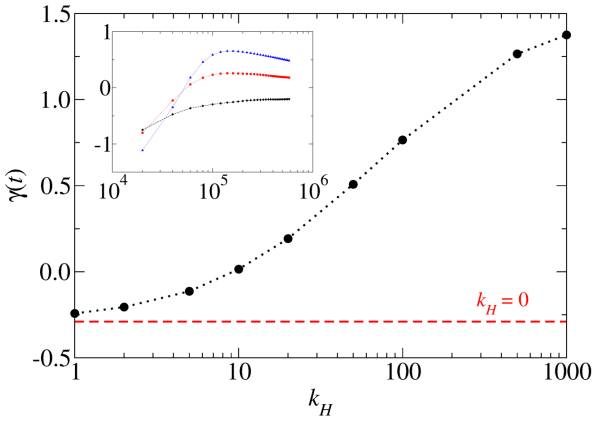

Figure 5: Skewness γ for the particle displacement distributions following the Henry adsorption isotherm as a function of k_H. Skewness data are plotted at a time corresponding to 500,000Δt. The red dashed line indicates the skewness for $k_H = 0$ (no adsorption). [Insert] Skewness γ as a function of time t for $k_H = 2$ (black), for $k_H = 20$ (red), and for $k_H = 50$ (blue).

3.2 Langmuir adsorption

We now discuss the transport of particles adsorbing according to the Langmuir adsorption isotherm. We consider the influence of different parameters such as the initial concentration c_0, the maximal surface saturation Γ^∞ and the Peclet number for a specific adsorption/desorption ratio: $k_L = 50$ (with $k_a = 0.05$ and $k_d = 0.001$). Further data for slow adsorption kinetics $k_L = 5$ (with $k_a = 0.005$ and $k_d = 0.001$) is given in the Supplemental Information file.

3.2.1 Influence of the initial concentration c_0

We first vary the initial concentration c_0 in the range $[10; 500]$ while setting the Peclet number $Pe = 19$ and surface saturation $\Gamma^\infty = 10$. Fig. 7 shows the normalized dispersion coefficient $D(t)/D_m$ [Top] for different c_0 together with the corresponding temporal evolution of the skewness $\gamma(t)$ [Bottom]. As reference data, $\gamma(t)$ for the passive, i.e. non-adsorbing, particles is also shown in the figure. For small c_0, an extended plateau for $D(t)/D_m$ is rapidly reached after a marked peak observed in the short time range.

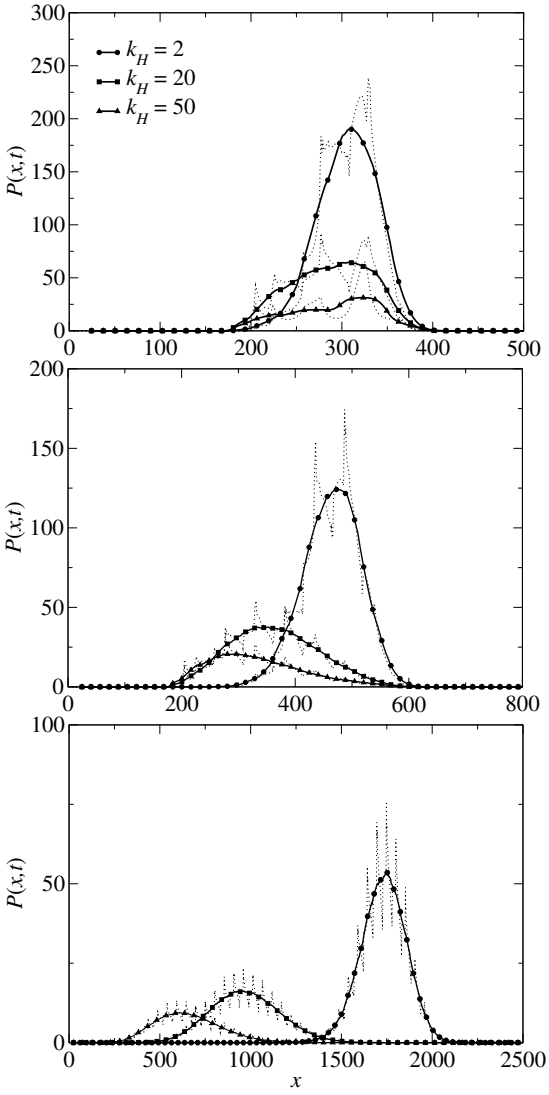

Figure 6: Propagators for transport under Henry adsorption conditions. The dashed curves correspond to propagators $P(x,t)$ divided by the local average porosity for $k_H = 2$, $k_H = 20$ and $k_H = 100$ at $t = 4 \times 10^4 \Delta t$ [Top], $10^5 \Delta t$ [Middle], $5.8 \times 10^5 \Delta t$ [Bottom]. The continuous curves are moving averages with 50 data-points. In all cases, the initial concentration is $c_0 = 10$ and the Peclet number is $Pe = 19$.

In contrast, while we expect a similar behavior for larger c_0, $D(t)/D_m$ also attains a maximum but for much larger times. Then, $D(t)/D_m$ decreases at a lower rate so that it does not fully reach the plateau regime on the time scale considered in the present calculations. The peak observed at short time, which is due to adsorption effects, occurs shortly after injection; the

system subdivides into two populations (i.e. adsorbed and free particles) on such timescales, therefore leading to a large dispersion coefficient arising from marked differences in the corresponding mean square displacements. On the other hand, in the long time limit, $D(t)/D_m$ reaches a plateau as all particles significantly exchange between adsorbed/desorbed states so that mean square displacements become more homogeneous.

The marked transport differences upon varying c_0 can be rationalized by monitoring the skewness $\gamma(t)$. For small c_0, $\gamma(t)$ is initially negative but rapidly becomes positive. Like for the Henry regime discussed earlier, this non-monotonous regime can be understood by invoking dominant geometrical heterogeneities in the short time scale (negative skewness due to strong flow path heterogeneities) which get counterbalanced by adsorption effects in the long time scale (positive skewness due to anti-tailing as a large part of the molecules get adsorbed over non negligible times). As expected, for small c_0, transport under Langmuir adsorption conditions is very similar – at least from a qualitative viewpoint – to transport under Henry conditions. Indeed, for small c_0, surface saturation inherent to Langmuir adsorption does not affect the results so that the mechanisms at play are essentially identical to those observed with Henry adsorption. In contrast, for large c_0, the skewness γ is negative as adsorption effects are limited due to surface saturation. Moreover, for large c_0, even at large times t, γ remains below the data observed for passive tracers. Such persistent effects can be explained by the fact that only a limited part of the molecules injected through the initial concentration c_0 gets adsorbed due to surface saturation (i.e. Langmuir adsorption regime). As a result, despite the large adsorption/desorption ratio k_H considered here, most particles remain free (desorbed) so that skewness remains mostly governed by flow paths heterogeneities (negative skewness). This interpretation is confirmed by the fact that the skewness $\gamma(t)$ at a given time gets more and more negative as c_0 increases and, hence, surface saturation becomes dominant.

In all cases, the absolute value of the skewness decreases in time as the effect of the injection condition fades out when all particles sample efficiently the adsorbed and non-adsorbed states. Typically, dynamic equilibrium between adsorbed and non-adsorbed particles is reached after a specific time t_{eq}. However, as can be seen from Fig. 7 [Bottom], this transient regime can last over very long times – especially for low c_0 where t_{eq} is found to exceed by far the typical simulation time. As expected, when observed within the typical simulation time considered here, the plateau value for $D(t)/D_m$ in the long time limit is found to increase with increasing c_0. This is due to the fact adsorption effects increase with c_0 as an increasing number of particles gets adsorbed.

3.2.2 Influence of surface saturation Γ^∞

In order to investigate the impact of surface saturation Γ^∞, we consider transport at constant initial concentration $c_0 = 500$ and Peclet number is $Pe = 19$. Identically, as in the previous section, the adsorption/desorption ratio is set to $k_L = 50$. Fig. 8 shows the normalized dispersion coefficient $D(t)/D_m$ [Top] together with the corresponding skewness $\gamma(t)$ [Bottom] for different surface saturation parameters Γ^∞. For large Γ^∞, $D(t)/D_m$ reaches rapidly a plateau after a short peak. This is due to the fact that adsorption occurs very fast without being limited by surface site availability; as a result, sampling between the adsorbed and desorbed states is efficient so that the asymptotic regime is reached quickly after injection. In contrast, for small Γ^∞, a strong increase in $D(t)/D_m$ can be observed followed by a decrease towards the plateau at the end of the simulation. Such a peak can be explained by the existence of two subpopulations in the short time range where one subpopulation is adsorbed rapidly after injection whereas the other subpopulation is transported by the Stokes velocity field. Yet, like the data observed for large Γ^∞, in the long time regime, particles sample both the adsorbed and non-adsorbed states efficiently so that the displacement distribution becomes Gaussian. In more

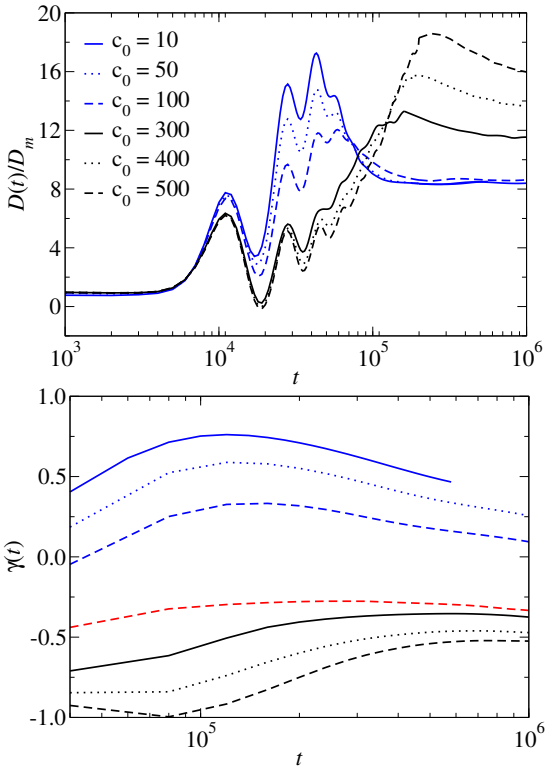

Figure 7: Transport under Langmuir adsorption conditions for different initial concentrations c_0. All calculations are performed with $k_L = 50$, $\Gamma^\infty = 10$ and $Pe = 19$. The dispersion coefficient $D(t)$ for different initial concentrations c_0 is presented in the top figure where $D(t)$ is normalized by the molecular diffusion coefficient D_m of the free, i.e. non-adsorbing, tracer particles [Top]. The corresponding skewness $\gamma(t)$ is shown in the bottom figure with the data for the passive tracer in red [Bottom].

detail, for small surface saturations, the typical time needed to reach the Gaussian regime becomes longer as fewer adsorption sites are available. In other words, particles remain for longer times in the bulk phase where they are transported by Stokes velocity field. As a result, the time to sample a significant number of adsorbed and non-adsorbed positions is larger so that $D(t)/D_m$ attains a plateau only at longer times.

As shown in Fig. 8, the skewness $\gamma(t)$ is negative for small Γ^∞ but positive for large Γ^∞. These results are consistent with those reported in the previous section on the impact of the initial concentration c_0. Typically, the positive skewness observed for large Γ^∞ can be explained by the fact that in this regime strong adsorption effects lead to anti-tailing (similarly, we observed such a positive skewness for small initial concentrations c_0 where adsorption effects are important as surface saturation does not affect adsorption/transport). In contrast, the negative skewness observed for small Γ^∞ is due to the fact that surface saturation limits adsorption so that a large number of free particles are transported by Stokes velocity field. Overall transport in this case is mostly governed by flow path heterogeneities, therefore leading to a nearly Gaussian-type concentration front but with negative skewness. Interestingly, upon reducing the surface saturation Γ^∞, we see in Fig. 8 that the time t_{eq} at which the plateau for $D(t)/D_m$ is reached increases. This is due to the fact that small Γ^∞ requires much longer times to sample efficiently both the adsorbed and desorbed states.

3.2.3 Influence of Peclet number Pe

We now compare the transport of particles following Langmuir adsorption conditions for different Peclet numbers: $Pe = 19$, $Pe = 9.5$ and $Pe = 3.8$. The surface saturation is set to $\Gamma^\infty = 1$ and the initial concentration $c_0 = 500$. In this case, all simulations are done for slow adsorption kinetics i.e. $k_L = 5$ in order to focus on the short-time transient regimes. Fig. 9 [Top] shows the normalized dispersion coefficient $D(t)/D_m$ for the three Peclet numbers. As shown in the previous section, $D(t)/D_m$ increases with time in the short time range as adsorption induces significant displacement differences between adsorbed and desorbed particles. In addition, as expected from such adsorption effects, the increase in $D(t)/D_m$ in this increasing regime is more pronounced for large Peclet numbers; this is due to the fact that differences between the transport of free and adsorbed particles become more important at large Peclet numbers. These results suggest that the non-Gaussian intermediate transport regime becomes more important for large Peclet numbers. However, when plotting the corresponding propagators at $t_0 = 8 \times 10^5 \Delta t$, $2t_0$ and $5t_0$ (see Fig. 9 [Bottom]), it can be seen

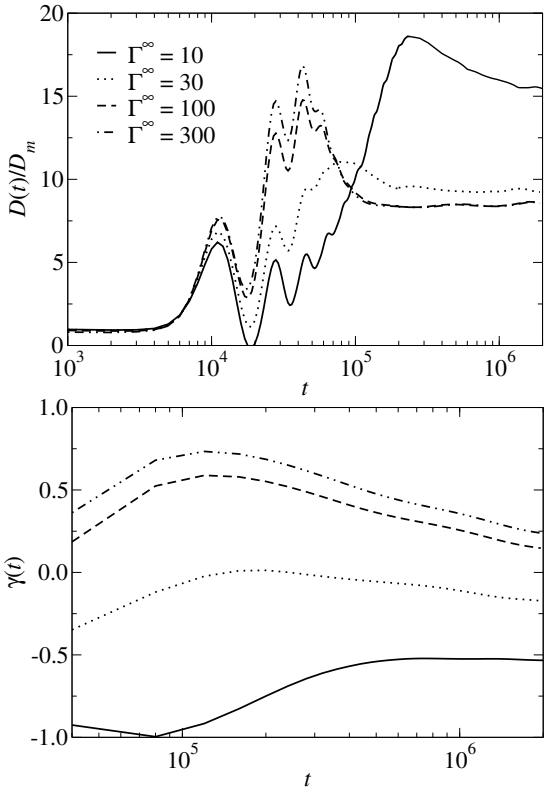

Figure 8: Transport under Langmuir adsorption conditions for different surface saturation Γ^{∞}. All calculations are performed with $k_L = 50$, $c_0 = 500$ and $Pe = 19$. The dispersion coefficient $D(t)$ is represented in the top figure where $D(t)$ is normalized by the molecular diffusion coefficient D_m of the free, i.e. non-adsorbing, particles [Top]. The corresponding skewness $\gamma(t)$ is shown in the bottom figure [Bottom].

that propagators do not significantly differ. In fact, the positions of the main peak are very close to each other while the shape of the propagator differs – with the distribution width being larger upon decreasing Pe. This finding is due to the fact that, upon increasing Pe, overall transport is mostly governed by the Stokes flow field. On the other hand, upon decreasing Pe, adsorption effects largely impact overall transport with important effects on the corresponding propagators. These results can be explained by considering the different time scales characterizing adsorption/diffusion and velocity/transport. On the one hand, slow velocity fields lead to dominant adsorption effects as it allows perpendicular diffusion of the particles towards the surface. On the other hand, fast velocity fields hinders such perpendicular diffusion towards the surface as particles are carried away by the fluid (leading to lower adsorption effects).

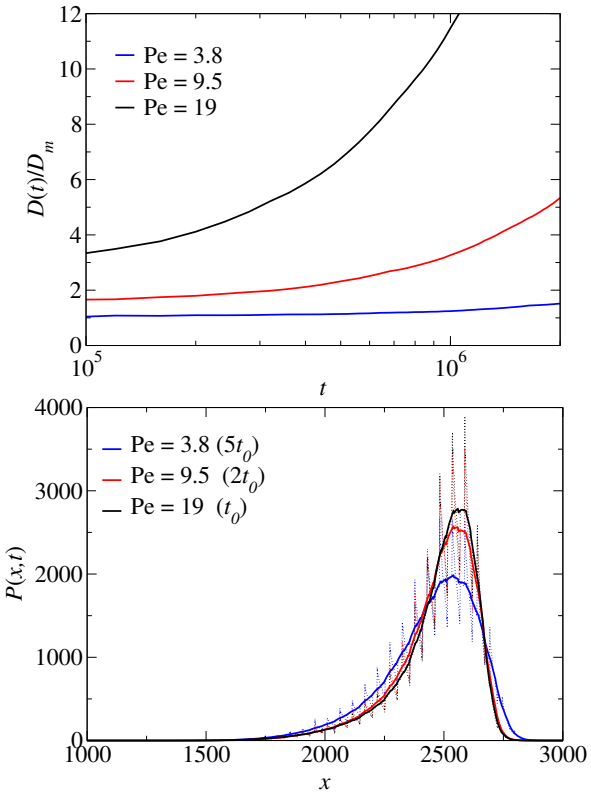

Figure 9: Transport under Langmuir adsorption conditions for different Peclet numbers. All calculations are performed with $k_L = 5$, $c_0 = 500$ and $\Gamma^{\infty} = 1$. The dispersion coefficient $D(t)$ is represented in the top figure where $D(t)$ is normalized by the molecular diffusion coefficient D_m of the free, i.e. non-adsorbing, particles [Top]. Propagators divided by the local average porosity are given at time $t_0 = 8 \times 10^5 \Delta t$, $2t_0$ and $5t_0$ [Bottom].

4 Conclusion

In this work, numerical simulations were used to study the coupling between adsorption and transport in a two-dimensional model of porous media. These simulations were performed using a Lattice Boltzmann approach extended to adsorption phenomena within the Two Relaxation Time framework – which ensures obtaining accurate and stable results in complex structures.

We focused on two specific adsorption models: (1) the Henry model in which the adsorbed amount scales linearly with the adsorbate free concentration in the fluid and (2) the Langmuir model which involves a maximal adsorbed concentration to include physical surface saturation. We considered the influence of these specific adsorption behaviors on overall transport. To this goal, we varied the following system parameters: adsorption/desorption ratio k, initial concentration c_0, surface saturation Γ^∞ and Peclet number Pe.

Transport regimes For all simulations, we observed three transport regimes. In the short time range, transport is dominated by diffusion. In the intermediate time range, the diffusion-dominated regime is followed by a transient regime controlled either by advection or adsorption phenomena. In the long time range, an effective Gaussian dispersion regime is observed. Our results show that the time evolution of the intermediate transient regime strongly depends on the adsorption kinetics but also on the system's parameters. In all cases, in the long time limit, provided particles sample sufficiently the adsorbed and non-adsorbed states, the influence of the initial state attenuates; as a result, at equilibrium, in the asymptotic limit, transport becomes Gaussian. However, the effective dispersion coefficient D_{eff} as well as the time to attain the asymptotic limit drastically depend on the adsorption model and system's parameters so that it might exceed by far the actual simulation time. Such findings shed light on numerous experimental situations where dispersion is found to remain anomalous (non-Gaussian) even if transport is considered over long macroscopic times.

Henry adsorption Particles following the Henry adsorption model are strongly adsorbed after injection as there is no surface saturation with this ideal model. Such rapid adsorption leads to strong separation of the particles into two subpopulations: adsorbed and non-adsorbed particles. While the adsorbed particles remain close to the inlet (injection region), the non-adsorbed particles are efficiently transported through the Stokes velocity field. This leads to a maximum in the normalized dispersion coefficient $D(t)/D_m$ during the transient regime. With such strong initial adsorption, the skewness $\gamma(t)$ – which characterizes the asymmetry in the concentration field – is positive in the transient regime and increases with the adsorption/desorption ratio k_H. This transient regime evolves towards a stationary behavior once particles have sampled sufficiently the adsorbed and non-adsorbed states (in that case, $D(t)/D_m$ decreases and reaches a plateau).

Langmuir adsorption kinetics Transport of particles following the Langmuir adsorption isotherm strongly depends on the initial concentration c_0 and surface saturation Γ^∞. As observed for the Henry adsorption model, the intermediate, i.e. transient, regime is drastically influenced by the system's parameters. For small c_0, transport is similar to that observed for Henry adsorbing particles as a large part of the particles gets adsorbed instantaneously after injection. However, for large c_0, advection in combination with adsorption dominates the transport behavior as only a limited part of the injected particles gets adsorbed. Both behaviors can also be observed in the skewness, which is positive in the first case and negative in the second case. Considering surface saturation Γ^∞, $D(t)/D_m$ attains a plateau after a transient peak for large Γ^∞ (this behavior is similar to that of particles following Henry adsorption). However, for small Γ^∞, the evolution $D(t)/D_m$ resembles that observed for large c_0.

In conclusion, we have shown that the type of adsorption model (with or without surface saturation) and the corresponding system's parameters strongly influence the transient transport regimes and, hence, the time to reach Gaussian, asymptotic dispersion. Our findings point to the need to include specific adsorption kinetics into transport models to derive a physically consistent picture of the temporal and spatial adsorption/transport behavior in porous media.

It is interesting to connect our findings to available experiments on the transport of adsorbing molecules in porous media. Such data are often obtained by performing column experiments,[25–28] where the so-called breakthrough curve, corresponding to the outlet concentration as a function of time, is evaluated to ob-

tain information on transport and adsorption parameters. The latter can be done by fitting analytical solutions to the experimental data.[29] However, several aspects often render this interpretation based on well-known ideal models difficult and, sometimes, inappropriate. In contrast, while the findings reported in the present paper must be further investigated, they are needed to help rationalize available experimental data which fail to obey established asymptotic regimes. Pore and network heterogeneity as well as adsorption influence the shape of the breakthrough curve, therefore making the determination of the adsorption parameters complicated. In particular, non-symmetric breakthrough curves with important tailing are difficult to evaluate and usually require further experiments to be performed using passive tracer – to separate adsorption effects from heterogeneity effects.[30] Moreover, significant noise and uncertainty in the experimental data can make their evaluation/interpretation in the short and long time range complex. Interpretation failure with classical models can also be associated with a limited column length as breakthrough curves are known to strongly depend on this parameter.[27,28] For short column lengths, the asymptotic regime is not reached and a specific analytical solution[29] should be used in this case. In this context, the findings such as those reported in the present paper can be used to derive a general framework taking into account transient regimes which are prone to occur in finite (small) samples. Such theoretical results can also help for the interpretation of data obtained using sophisticated experimental techniques (e.g. MRI,[31] microtomography,[32] micromodel,[33] dichromatic X-Ray spectrometer[34]). These methods allow, in addition to determining breakthrough curves, the acquisition of spatial and/or temporal concentration profiles. Such data, which are relevant to transient and stationary transport regimes (e.g. preasymptotic and asymptotic) allow measuring complex concentration profiles evolving from non-Gaussian towards Gaussian.[34] Also, accumulating concentration profiles and breakthrough curves permits better parameter identification. Nevertheless, although these techniques are very efficient for certain types of molecules, their inherent measuring principle cannot be applied to all types of molecules so that additional theoretical treatment is needed. In addition, even very homogeneous, natural porous media (e.g. sandpacks) show a long lasting preasymptotic regime due to the slight disorder of the structure.[35] Therefore, a systematic, broad-range parameter study taking into account transient regimes to evaluate the coupling between transport and adsorption thermodynamics in the different regimes is experimentally very difficult.

In future work, it seems crucial to focus on the coupling between transport/adsorption and the heterogeneity inherent to real porous media. The velocity field in heterogeneous porous media includes high and low velocity zones that depend on the local structure. Thus, the transport behavior becomes more complex as spatially heterogeneous adsorption behaviors are expected. Indeed, structure heterogeneity implies that a large range of characteristic times in the velocity field competes with the characteristic times for adsorption. Therefore, further knowledge on the macroscopic transport equations seems to be crucial in order to correctly describe transport at a larger scale.

Supplemental Information The following Supplemental Information is available free of charge at the ACS website:

- Standard Lattice Boltzmann scheme for the resolution of Stokes equation
- Results of the Langmuir simulations for $k_l = 5$

Acknowledgment Zaineb Zaafouri acknowledges Ph.D. funding at Univ. Grenoble Alpes from IFP Energies Nouvelles.

References

(1) Wu, T.; Zhang, D. Impact of Adsorption on Gas Transport in Nanopores. *Sci. Rep.* **2016**, *6*, 1–10.

(2) Ichikawa, Y.; Selvadurai, A. *Transport Phenomena in Porous Media, Aspects of Micro/Macro Behaviour*; Springer, 2012.

(3) Bear, J. *Modeling Transport of Chemical Species*; Springer, 2018.

(4) Roque-Malherbe, R. *Adsorption and Diffusion in Nanoporous Materials*; CRC Press, 2018.

(5) Coasne, B. Multiscale adsorption and transport in hierarchical porous materials. *New J. Chem.* **2016**, *40*, 4078–4094.

(6) Levesque, M.; Duvail, M.; Pagonabarraga, I.; Frenkel, D.; Rotenberg, B. Accounting for adsorption and desorption in lattice Boltzmann simulations. *Phys. Rev. E* **2013**, *88*, 1–6.

(7) Vanson, J.-M.; Coudert, F.-X.; Rotenberg, B.; Levesque, M.; Tardivat, C.; Klotz, M.; Boutin, A. Unexpected coupling between flow and adsorption in porous media. *Soft Matter* **2015**, *11*, 6125–6133.

(8) Vanson, J.-M.; Coudert, F.-X.; Klotz, M.; Boutin, A. Kinetic accessibility of porous material adsorption sites studied through the Lattice Boltzmann Method. *Langmuir* **2017**, *33*, 1405–1411.

(9) Vanson, J.-M.; Boutin, A.; Klotz, M.; Coudert, F.-X. Transport and adsorption under liquid flow: the role of pore geometry. *Soft Matter* **2017**, *13*, 875–885.

(10) Coasne, B.; Galarneau, C., Anne andGerardin; Fajula, F.; Villemot, F. Molecular Simulation of Adsorption and Transport in Hierarchical Porous Materials. *Langmuir* **2013**, *29*, 7864–7875.

(11) Galarneau, A.; Guenneau, F.; Gedeon, A.; Mereib, D.; Rodriguez, J.; Fajula, F.; Coasne, B. Probing Interconnectivity in Hierarchical Microporous/Mesoporous Materials Using Adsorption and Nuclear Magnetic Resonance Diffusion. *J. Phys. Chem. C* **2016**, *120*, 1562–1569.

(12) Hlushkou, D.; Gritti, F.; Guiochon, G.; Seidel-Morgenstern, A.; Tallarek, U. Effect of Adsorption on Solute Dispersion: A Microscopic Stochastic Approach. *Anal. Chem.* **2014**, *86*, 4463–4470.

(13) Miura, T.; Seki, K. Diffusion Influenced Adsorption Kinetics. *J. Phys. Chem.* **2015**, *119*, 10954–10961.

(14) Chen, Y.; Shen, C.; Pengfei, L.; Huang, Y. Role of pore structure on liquid ow behaviors in porous media characterized by fractal geometry. *Chem. Eng. Process* **2015**, *87*, 75–80.

(15) Noetinger, B.; Roubinet, D.; Dreuzy, J.-R. d.; Russian, A.; Gouze, P.; Le Borgne, T.; Dentz, M.; Delay, F. Random walk methods for modeling hydrodynamic transport in porous and fractured media from pore to reservoir scale. *Transp. Porous Media* **2016**, *115*, 345–385.

(16) Wei, M.; Liu, Y.; Liu, J.; Elsworth, D.; Zhou, F. Microscale investigation on coupling of gas diffusion and mechanical deformation of shale. *J. Pet. Sci. Eng.* **2019**, *175*, 961–970.

(17) Bousige, C.; Levitz, P.; Coasne, B. Bridging scales in disordered porous media by mapping molecular dynamics onto intermittent Brownian motion. *Nat. Comm.* **2021**, *12*, 1–11.

(18) Fagbemi, S.; Tahmasebi, P.; Piri, M. Interaction between fluid and porous media with complex geometries: a direct pore-scale study. *Water Resour. Res.* **2018**, *54*, 6336–6356.

(19) Zaafouri, Z.; Batôt, G.; Nieto-Draghi, C.; Rotenberg, B.; Bauer, D.; Coasne, B. Lattice Boltzmann method for adsorption under stationary and transient conditions: Interplay between transport and adsorption kinetics in porous media. *Phys. Rev. E* **2021**, *104*, 015314.

(20) Levesque, M.; Bénichou, O.; Voituriez, R.; Rotenberg, B. Taylor dispersion with adsorption and desorption. *Phys. Rev. E* **2012**, *86*, 036316.

(21) d'Humieres, D. Generalized lattice-Boltzmann equations. *Rarefied gas dynamics* **1992**,

(22) Lallemand, P.; Luo, L. Theory of the lattice Boltzmann method: Dispersion, dissipation, isotropy, Galilean invariance, and stability. *Phys. Rev. E* **2000**, *6546*.

(23) Ginzburg, I.; d'Humières, D.; Kuzmin, A. Optimal stability of advection-diffusion lattice Boltzmann models with two relaxation times for positive/negative equilibrium. *J. Stat. Phys.* **2010**, *139*, 1090–1143.

(24) Zaafouri, Z.; Batôt, G.; Nieto-Draghi, C.; Coasne, B.; Bauer, D. Impact of adsorption kinetics on pollutant dispersion in water flowing in nanopores: A Lattice Boltzmann approach to stationary and transient conditions. *Adv. Water Resour.* **2022**, *162*, 1–12.

(25) Dias Novaes, S.; Oliveira, P. V.; Siqueira Petri, D. F. Hydroxypropyl methylcellulose-sugarcane bagasse adsorbents for removal of 17-ethinylestradiol from aqueous solution and freshwater. *Environ. Sci. Pollut. Res.* **2002**, *76*, 88.

(26) Negrea, A.; Mihailescu, M.; Mosoarca, G.; Ciopec, M.; Duteanu, N.; Negrea, P.; Minzatu, V. Estimation on Fixed-Bed Column Parameters of Breakthrough Behaviors for Gold Recovery by Adsorption onto Modified/Functionalized Amberlite XAD7. *Int. J. Env. Res. Pub. He.* **2020**, *10*, 1–14.

(27) Biswas, S.; Mishra, U. Continuous Fixed-Bed Column Study and Adsorption Modeling: Removal of Lead Ion from Aqueous Solution by Charcoal Originated from Chemical Carbonization of Rubber Wood Sawdust. *Int. J. Chem.* **2015**, *907379*, 1–9.

(28) Lopez-Cervantes, J.; Sanchez-Machado, D.; Sanchez-Duarte, R.; Correa-Murrieta, M. Study of a fixed-bed column in the adsorption of an azo dye from an aqueous medium using a chitosan– glutaraldehyde biosorbent. *Adsorp. Sci. Technol.* **2018**, *36*, 1–18.

(29) Patel, H. Fixed-bed column adsorption study: a comprehensive review. *Applied Appl. Water Sci.* **2019**, *9*, 1–17.

(30) Wernert, V.; Nguyen, K. L.; Levitz, P.; Coasne, B.; Denoyel, R. Impact of surface diffusion on transport through porous materials. *J. Chromatogr. A* **2022**, *1665*, 1–12.

(31) Baer, N.-K.; Balcom, B.; Ruthven, D. Direct Measurement of Transient Concentration Profiles in Adsorbent Particles and Chromatographic Columns by MRI. *Ind. Eng. Chem. Res. 2* **2002**, *41*, 2320–2329.

(32) Lodewyckx, P.; Blacher, S.; Leonard, A. Use of x-ray microtomography to visualise dynamic adsorption of organic vapour and water vapour on activated carbon. *Adsorption* **2006**, *12*, 19–26.

(33) de Vries, E.; Tang, Q.; Faez, S.; Raoof, A. Fluid flow and colloid transport experiment in single-porosity sample; tracking of colloid transport behavior in a saturated micromodel. *Adv. Water Resour.* **2022**, *159*, 1–11.

(34) Latrille, C.; Neel, M.-C. Transport study in unsaturated porous media by tracer experiment in a dichromatic X-ray experimental device. *EPJ Web of Conferences* **2013**, *50*, 1–7.

(35) Guillon, V.; Fleury, M.; Bauer, D.; Neel, M.-C. Superdispersion in homogeneous unsaturated porous media using nmr propagators. *Phys. Rev. E* **2013**, *87*, 043007.